HHS Public Access

Author manuscript

Cytoskeleton (Hoboken). Author manuscript; available in PMC 2025 August 01.

Published in final edited form as:

Cytoskeleton (Hoboken). 2024 August ; 81(8): 356–368. doi:10.1002/cm.21849.

Microtubule length correlates with spindle length in *C. elegans* meiosis

Vitaly Zimyanin[1,2], **Stefanie Redemann**[*,1,2,3]

[1]Department of Molecular Physiology and Biological Physics, University of Virginia, School of Medicine, Charlottesville, VA, USA

[2]Center for Membrane and Cell Physiology, University of Virginia School of Medicine, Charlottesville, VA, USA

[3]Department of Cell Biology, University of Virginia School of Medicine, Charlottesville, VA, USA.

Abstract

The accurate segregation of chromosomes during female meiosis relies on the precise assembly and function of the meiotic spindle, a dynamic structure primarily composed of microtubules. Despite the crucial role of microtubule dynamics in this process, the relationship between microtubule length and spindle size remains elusive. Leveraging *C. elegans* as a model system, we combined electron tomography and live imaging to investigate this correlation. Our analysis revealed significant changes in spindle length throughout meiosis, coupled with alterations in microtubule length. Surprisingly, while spindle size decreases during the initial stages of anaphase, the size of antiparallel microtubule overlap decreased as well. Detailed electron tomography shows a positive correlation between microtubule length and spindle size, indicating a role of microtubule length in determining spindle dimensions. Notably, microtubule numbers displayed no significant association with spindle length, highlighting the dominance of microtubule length regulation in spindle size determination. Depletion of the microtubule depolymerase KLP-7 led to elongated metaphase spindles with increased microtubule length, supporting the link between microtubule length and spindle size. These findings underscore the pivotal role of regulating microtubule dynamics, and thus microtubule length, in governing spindle rearrangements during meiotic division, shedding light on fundamental mechanisms dictating spindle architecture.

Introduction

Female meiosis is a complex cellular process that involves two successive divisions, in which half of the chromosome content is extruded into two polar bodies, resulting in the formation of a haploid oocyte that is ready for fertilization. Errors in the segregation of chromosomes often lead to aneuploidy, an abnormal number of chromosomes, which has detrimental consequences for the development and survival of the oocyte. It is known that

[*]Corresponding author: sz5j@virginia.edu.

Authors Contribution

S.R. generated and analyzed the light- and electron microscopy data, V.Z. helped with conceptualization and co-wrote the paper.

Conflict of Interest

No, there is no conflict of interest

misregulation of microtubule dynamics disrupts meiosis (1,2). However, the mechanisms that explain this observation have remained opaque.

During the meiotic divisions, the segregation of chromosomes is mediated by the meiotic spindle, a self-assembling, dynamic structure composed of microtubules, motor proteins, microtubule binding proteins, and various regulatory factors. Unlike other spindles in most animals, female meiotic spindles typically have no centrosomes, due to centriole elimination during oogenesis. Thus, female meiotic spindles must assemble and segregate chromosomes without centriole containing microtubule organizing centers. Specifically, this is true in humans (3), mice (4) and also in nematodes (5). The assembly and regulation of meiotic spindles involves multiple stages, including microtubule nucleation, organization and stabilization, as well as the coordination of motor protein activity and regulatory signaling. While much is known about the role of motor proteins and regulatory signaling (6–9) in meiosis, comparatively less is known about the role and importance of microtubule dynamics during meiotic spindle formation and chromosome segregation (10), even though dynamic microtubules are the main building blocks of spindles. Several publications showed that the microtubule severing protein katanin plays an important role in meiotic spindles by regulating microtubule length, turnover dynamics, and organization. Katanin's ability to sever microtubules contributes to spindle remodeling, ensuring the proper assembly, function, and reorganization of the meiotic spindle during cell division (11–16). While it is known that microtubules turn over at high rates in spindles, and that this can generate forces and modify the overall connectivity of the spindle (17), it has remained elusive how this process is regulated and how it contributes to essential spindle functions such as chromosome congression and chromosome segregation in anaphase.

Specifically for meiotic divisions previous research has shown that microtubule growth dynamics are crucial for correct meiotic spindle formation and function, as treatment of mouse oocytes with taxol impairs microtubule and chromosome organization as well as meiotic progression and leads to aneuploidy (1). Further, mutations or disruptions in proteins involved in the regulation of microtubule dynamics, such as XMAP215/Dis1 family proteins (18–22) and their regulators or MCAK (23–26) result in abnormal spindle structures, misaligned chromosomes, and failed chromosome segregation in yeast, Drosophila, mice and various other organisms. In addition, oocytes from older mice exhibit altered spindle microtubule dynamics which may contribute to age-related increases in chromosome segregation errors that are observed in these animals (2). These findings highlight the critical role of microtubule dynamics in establishing functional meiotic spindles and ensuring accurate chromosome segregation.

One of the main obstacles in identifying the role of microtubule dynamics during meiosis is the limitation of light microscopy in resolving submicron structures. Thus, information such as the number and length of microtubules, their interactions with chromosomes, their nucleation pattern and conformation cannot be obtained by light microscopy and is only inferred from indirect measurements. To overcome these shortcomings, we are using 3D electron reconstructions of spindles in *C. elegans* (27–30). *C. elegans* has been extensively used as a model system to understand chromosome segregation in meiotic and mitotic

spindles, especially since most of the proteins involved in meiotic divisions in *C. elegans* have orthologues in humans (31).

Our previously generated reconstructions of complete spindles in *C. elegans* oocytes in different stages of meiosis I and II by 3D electron tomography revealed that these spindles are mainly composed of an array of short microtubules with nearly half of them being shorter than 500 nm (32). It also showed that there are significant changes in microtubule number and length throughout meiosis, with the number of microtubules doubling from metaphase to early anaphase and then reducing again by 2-fold in mid-anaphase. This change in microtubule number is consistent with light microscopy observations that microtubules are highly dynamic in meiosis, with turn-over rates of approximately ~ 5s and a rapid poleward movement with a rate of 8.5 ± 2.2 μm/min (32). Overall, our data suggested that regulation of microtubule dynamics, such as nucleation rate, growth and catastrophe rates, leading to changes in microtubule numbers and length might be involved in transitioning through meiosis.

In this study we combine static, yet spatially resolved, ultrastructural data obtained by electron tomography with dynamic data from light microscopy to further determine which microtubule parameters and changes in organization could be critical for the rearrangement of the meiotic spindle structure throughout meiosis in the *C. elegans* oocyte.

Results

The microtubule overlap in the meiotic spindle decreases throughout anaphase

Live imaging of meiotic spindles during both meiotic divisions shows significant changes in the structure and size of the spindle throughout meiosis (Fig. 1). At metaphase of meiosis I, the average size of the meiotic spindle is 3.4μm± 0.1μm (SEM, n=7), it shortens significantly throughout the first ~80 s of anaphase (2.1μm± 0.2μm (n=7)) and then increases in size during chromosome segregation while further progressing through anaphase (3.4μm± 0.4μm (n=7) (Fig, 1A, timepoint ‘0’ is anaphase onset, defined as the first frame with visible chromosome separation). The meiotic spindle undergoes similar changes in meiosis II, where the average spindle size decreases from 3.9μm± 0.4μm (SEM, n=6) in metaphase to 2μm± 0.2μm (n=6) in early stage of anaphase and 3.1μm± 0.2μm (n=6) in late anaphase (Fig. 1B). This data shows that the meiotic spindle undergoes significant changes in length throughout meiosis, consistent with previous studies (33,34), and raises the question of how these changes are regulated.

One possible hypothesis is that motor proteins could drive an initial inward sliding of microtubules in early stages of anaphase and thus lead to a decrease in spindle length. We speculate that such behavior could affect the region of antiparallel microtubule overlap in the spindle midzone, the region between the chromosomes during anaphase. The spindle midzone has been shown to actively participate in chromosome segregation and spindle elongation in mitosis and meiosis (35) presumably by generating outward directed forces. Our data on mitotic cells showed that the overlap between antiparallel microtubules remained surprisingly stable (36) throughout anaphase suggesting that microtubules within

this overlap must either polymerize or be constantly rearranged to maintain the antiparallel overlap while the spindle midzone extends.

To obtain further insight into the structure of the midzone throughout meiosis that could regulate the changes in spindle length we quantified the microtubule arrangement in the spindle midzone. We used second harmonic generation (SHG) microscopy and two photon fluorescence (TP) microscopy simultaneously to measure the polarity of the collective microtubules throughout the spindle in vivo (37) (Fig. 2A). Surprisingly this data showed that the antiparallel overlap of microtubules within the meiotic spindle became smaller from metaphase to anaphase, while the spindles shortened (Fig. 2B). In agreement with this we previously found that microtubules in the spindle midzone in meiosis are sliding apart with similar velocities as the chromosomes (35). While the antiparallel microtubule region decreases throughout anaphase, we found that the microtubule overlap always extended for about 20% of the spindle length when the data was normalized by spindle length. Although the decrease in microtubule overlap is consistent with the midzone playing an active role in chromosome segregation and the generation of outward directed forces, it does not explain the observed decrease in spindle length throughout the initial stages of anaphase.

To establish which characteristics of microtubules change during the re-arrangement of meiotic spindles we used 3 D electron tomography to obtain detailed information about microtubule organization in meiotic spindles throughout meiosis I and II.

We previously reconstructed six meiosis I and four meiosis II (Fig. 3A,B) spindles at different stages throughout cell division (32,38). In agreement with the light microscopy data the reconstructed spindles show similar changes in spindle length throughout meiosis, with spindles shrinking from metaphase to early anaphase and then increasing in length while anaphase progresses (Fig. 3C top). These changes in size are accompanied by changes in microtubule number (Fig. 3C middle) and length (Fig. 3C bottom), where spindles in early anaphase that were presumably shortening showed increased microtubule numbers and decreased microtubule length (Fig.3C). We also used the tomographic data to determine the microtubule polarity along the spindle (Fig. 3D). As the polarity of microtubules can not be determined in the tomographic data we assigned polarities to the microtubules, depending on their closest distance to one of the spindle poles (see inset in Fig, 3D showing blue and yellow microtubules). The plot of microtubule polarity along the spindle length using this methodology (Fig. 3D) looked very similar to the plot we obtained by combined SHG and TP imaging (Fig. 2), suggesting that the antiparallel microtubule overlap region decreases over time.

Microtubule length correlates with the spindle size throughout meiosis.

To further determine changes in microtubule properties that could affect spindle length, we used the detailed data obtained by electron tomography to determine potential correlations between spindle length and microtubule number, average microtubule length, total polymer length (the added length of all microtubules in the spindle) and chromosome volume. In total we re-visited 10 complete spindles, 6 in meiosis I and 4 in meiosis II, with an average of ~3500 microtubules each. While this is a rather small sample size this data still provides

valuable insights into potential correlations. For this analysis, we initially pooled that data of meiosis I and II to have a larger sample size.

Quantification of the data suggest that the number of microtubules ($r=0.84$, $p<0.05$) in a spindle as well as the average length of microtubules ($r=0.62$, $p<0.05$) positively correlate with the total polymer length of microtubules (Fig. 4 A,B,H). However, we could not show a correlation between microtubule length and microtubule number ($r=0.12$) (Fig. 4C,H). Our data also showed that there is no correlation between the microtubule number and the spindle length ($r=0.07$) (Fig. 4D,H), as well as between the total Chromosome Volume and the spindle length ($r=-0.29$, ns) in meiosis (Fig. 4E,H). Spindle length was only weakly and not significantly correlated with the total polymer length ($r=0.46$, ns) (Fig. 4G,H). Most strikingly our data revealed that there was a positive correlation between the average microtubule length and the spindle length ($r=0.79$, $p<0.05$) (Fig. 4 F,H) through meiosis.

Individual quantification of meiosis I and II showed similar results (Suppl. Fig. 1, 2). The number of microtubules correlated positively with the total polymer length in meiosis I (Suppl. Fig.1A,H, $r= 0.85$, $p<0.05$) and II datasets (Suppl Fig.2A,H, $r= 0.89$, $p<0.05$). However, we could no longer detect a correlation between microtubule length and polymer length (Suppl. Fig 1B,H, Suppl. Fig. 2B, H). The individual quantifications also showed a a positive correlation between the average microtubule length and the spindle length in meiosis I (Suppl. Fig. 1F, H, $r= 0.75$, $p<0.05$) and II (Suppl. Fig. 2F, H, $r= 0.95$, $p<0.05$). Interestingly, the data for meiosis I also showed a negative correlation between chromosome volume and spindle length (Suppl. Fig. 1E, H, $r= -0.83$, $p<0.05$). We also detected a negative correlation of chromosome size and spindle length in meiosis II, but it was not significant (Suppl, Fig. 1E, H, $r=-0.75$, ns). Our data also showed that there is no correlation between the microtubule length and microtubule number, microtubule number and spindle length and Polymer length and spindle length in meiosis I (Suppl. Fig. 1C,D,G,H) and II (Suppl. Fig. 2C,D,G,H).

In summary this data suggests that the average length of microtubules affects the spindle size and that microtubule dynamics are a more critical parameter in regulating spindle size. On the other hand, regulation of microtubule nucleation and thus microtubule numbers might play a less important role in meiosis. The data also suggests that Chromosome volume could affect spindle length as has been previously suggested by other groups (39–41).

Longer meiotic spindles are composed of longer microtubules

To further test the hypothesis that elongation of spindles corresponds to an overall increase in microtubule length, we quantified the effect of depletion of the microtubule depolymerase KLP-7. As a member of the kinesin-13 family, the *C. elegans* MCAK homolog KLP-7 possesses microtubule-depolymerizing activity, allowing it to selectively remove tubulin subunits from microtubule ends (42). This unique ability enables KLP-7 to influence microtubule length and stability. Previous research has shown that KLP-7 is required for bipolar oocyte meiotic spindle assembly. In absence of KLP-7, extra microtubules accumulate often leading to the formation of additional functional spindle poles assembled during meiosis I anaphase (43). This data suggested a role for KLP-7 in preventing ectopic, spontaneous microtubule assembly (44). Previous data from our lab also supported these

observations by showing that KLP-7 is required to remove laterally associated microtubules around chromosomes during meiosis (38)

Analysis of meiotic spindles by light microscopy showed that KLP-7 depleted spindles do not display a shortening of the meiotic spindles during early anaphase in meiosis I, leading to overall longer spindles in early anaphase, with 2.1μm ± 0.2μm (n=7) in control vs 4.4μm± 0.4μm (n=4) after *klp-7 (RNAi)* at 80s after anaphase onset (Fig. 5A,B). We quantified two 3D tomographic reconstructions after *klp-7 (RNAi)*, one of a spindle in metaphase of meiosis I, which is elongated in comparison to control conditions, and one in anaphase of meiosis I, which is similar in size to control conditions (Fig. 5C). We plotted the data for those two spindles together with the data for meiosis I and II correlating spindle length with average microtubule length. For both of the *klp-7 (RNAi)* data sets the average microtubule length is indicative of spindle length (Fig. 5D). In particular, the elongated metaphase spindle (9μm, Fig. 5C top) also has an increased average microtubule length (1.25 μm ± 0.03μm) in comparison to control metaphase spindles. This results supports our observation that spindle size is affected by microtubule length. Given the molecular function of KLP-7 this result suggests that regulation of microtubule dynamics and thus controlling microtubule length is an important molecular mechanism that regulates spindle size in *C. elegans* meiosis.

Discussion.

Female meiosis is crucial for the formation of a viable oocyte and the precise chromosome segregation facilitated by the meiotic spindle is essential. Errors in this process often result in aneuploidy, underscoring the significance of understanding the underlying mechanisms governing meiotic spindle dynamics. Combining ultrastructural insights from electron tomography with dynamic observations from light microscopy, we aimed to identify microtubule parameters that might affect spindle morphology throughout the *C. elegans* oocyte division.

The meiotic spindle undergoes distinct changes in spindle size throughout meiosis, characterized by a notable shortening during early anaphase followed by elongation as anaphase progresses. This pattern is consistent across both meiotic divisions, underscoring the dynamic nature of spindle architecture throughout oocyte division.

Assessing the microtubule overlap within the spindle midzone using second harmonic generation microscopy and two-photon fluorescence microscopy shows a reduction in antiparallel microtubule overlap from early anaphase throughout anaphase. This contrasts with our recently reported analysis of microtubule overlap in mitotic spindles, which remains constant throughout anaphase. However, our data on meiotic spindles shows that despite spindle size changes, the fraction of the antiparallel overlap region in comparison to the full spindle length remains relatively constant, implying some mechanism of overlap regulation during meiosis. Overall, this data suggests that alternative mechanisms might be at play regulating spindle length beyond changes in microtubule overlap.

Direct measurements of microtubule properties via electron tomography provide crucial insights into the potential correlation between microtubule properties and spindle length. Our analysis indicates a positive correlation between the length of microtubules and the length of the spindles at different stages. Intriguingly, while microtubule length positively correlated with spindle size, there was no significant correlation between microtubule number and spindle length. This highlights the pivotal role of microtubule length in determining spindle size. This observation agrees with previous data that suggested that modulation of microtubule dynamics, in particular growth rates and catastrophe frequency, provides an efficient mechanism to control spindle length during embryonic development (45–47). It was also suggested that those changes in microtubule dynamics would affect the length of microtubule and that varying microtubule dynamics sets an average microtubule length that scales with cell volume and spindle length (47). Our data strongly supports the hypothesis that microtubule length affects spindle length, and that this correlation is not only functioning during development but also during the progression through meiosis.

Further reinforcing the link between spindle length and microtubule dynamics, the depletion of the microtubule depolymerase KLP-7 resulted in elongated spindles during early anaphase in meiosis I. Analysis of tomographic reconstructions showed an increase in microtubule average length and thus supported our observation, suggesting a strong association between microtubule length and resultant spindle size.

In conclusion, our integrative approach combining electron tomography with live imaging delineates the pivotal role of microtubule dynamics in governing spindle rearrangements throughout meiotic division. These findings underscore the importance of microtubule length regulation in determining spindle size and emphasize the need for further exploration to comprehensively understand the intricate interplay between microtubule dynamics and spindle architecture.

Material and methods.

Worm strains gene silencing by RNAi

MAS91 (unc-119(ed3) III; ItIs37[pAA64; pie-1::mCherry::HIS58]; ruIs57[pie-1::GFP:: b-tubulin+unc-119(+)]) was used for experiments of fluorescence imaging, and fluorescence recovery after photobleaching. MAS91 was a gift from Martin Srayko.

Worms were cultured and maintained at 16°C as described (48). RNAi experiments were performed by feeding (49). The feeding clone for *klp-7* was obtained from the RNAi library (50). L4 larvae were transferred to plates seeded with bacteria producing dsRNA and grown for 24 h at 25°C prior to analysis.

Light microscopy

Sample preparation for light microscopy—Oocytes for live-cell imaging were prepared as described previously (51).

Spinning disk confocal fluorescence imaging—Live imaging was performed using a spinning disk confocal microscope (Nikon Ti2000, Yokugawa CSU-X1), equipped with 488-

nm and 561-nm diode lasers, an EMCCD camera (Hamamatsu), and a 60X water-immersion objective (CFI Plan Apo VC 60X WI, NA 1.2, Nikon). Acquisition parameters were controlled using a home-developed LabVIEW program (LabVIEW, National Instruments). Images were acquired every 20 seconds over 59 z-planes covering approximately 16.460μm.

Quantification of spindle length and chromosome distances—The measurements of chromosome distances and spindle length were performed on maximum intensity projections of the z-stacks. The chromosome distance was measured from center to center of each chromosome. The spindle length before metaphase and during early anaphase was measured from the outer edges of the tubulin signal. During later stages, when the chromosomes are segregating and form the outer boundary of the spindle, spindle length was measured from the outer edge of each chromosome. The timepoint '0' shown in Figures 1 and 5 refers to anaphase onset, the first frame with visible chromosome separation. In our quantifications metaphase is defined as the last frame before anaphase onset.

Sample preparation for electron tomography

Wild-type (N2) *C. elegans* embryos were collected in cellulose capillary tubes(52) and high-pressure frozen as described using an EM ICE high-pressure freezer (Leica Microsystems, Vienna, Austria)(53). Freeze substitution was performed over 2–3 d at −90°C in anhydrous acetone containing 1% OsO_4 and 0.1% uranyl acetate. Samples were embedded in Epon/Araldite and polymerized for 2 d at 60°C. Serial semi thick sections (200 nm) were cut using an Ultracut UCT Microtome (Leica Microsystems, Vienna, Austria) collected on Pioloform-coated copper slot grids and post stained with 2% uranyl acetate in 70% methanol followed by Reynold's lead citrate. For dual-axis electron tomography (Mastronarde 1997), 15 nm colloidal gold particles (Sigma-Aldrich) were attached to both sides of semi-thick sections to serve as fiducial markers for subsequent image alignment. A series of tilted views were recorded using an F20 electron microscopy (Thermo-Fisher, formerly FEI) operating at 200 kV at magnifications ranging from 5000× to 6500× and recorded on a Gatan US4000 (4000 px × 4000 px) CCD or a Tietz TVIPS XF416 camera. Images were captured every 1.0° over a ±60° range.

Quantification of electron tomography data

We used the IMOD software package (http://bio3d.colorado.edu/imod) for the calculation of electron tomograms(54). We applied the Amira software package for the segmentation and automatic tracing of microtubules(55). For this, we used an extension to the filament editor of the Amira visualization and data analysis software(29,56,57). We also used the Amira software to stitch the obtained 3D models in *z* to create full volumes of the recorded spindles(56,57). The automatic segmentation of the spindle microtubules was followed by a visual inspection of the traced microtubules within the tomograms. Correction of the individual microtubule tracings included manual tracing of undetected microtubules, connection of microtubules from section to section, and deletions of tracing artifacts (e.g., membranes of vesicles).

Estimated errors of the electron tomography data

In this and our previous datasets we estimated that potential errors of joining individual sections of the traced tomogram can result in about 2% of microtubule with unclear end points and does not significantly affect the length distribution analysis of microtubule (56).

Tomogram segmentation, tracing and stitching inadvertently introduces some mistakes due to some local distortions of the data during imaging and potential errors of tracing, section matching and stitching. Our estimates of automatic tracing error lies within 5–10% range and therefore all datasets are further manually checked for tracing errors in each section and after the section joining. Previous analysis of microtubule endpoint distribution does detect some reduction of values at the section boundaries. However, contribution of all these errors is very unlikely to significantly affect the bulk of the measurements parameter value that we analyze in this manuscript.

Data analysis for tomography

Data analysis was performed using the Amira software (Visualization Sciences Group, Bordeaux, France). The different stages of meiosis were determined visually based on spindle shapes and chromosome position. The spindle length was measured from the outer edges of the detected microtubules composing the spindle in metaphase and early anaphase, when chromosomes began to form the outer boundary of the spindle during anaphase, spindle length was quantified by measuring the distance between the outer edges of the chromatin mass.

Length distribution of microtubules: For the analysis of the microtubules length distributions, we previously found that removing microtubules that leave the tomographic volume only had minor effects on the length distribution(56). Therefore, we quantified all microtubules contained in the volume. In addition, in all analyses, microtubules shorter than 100 nm were excluded to reduce errors due to the minimal tracing length.

Total polymer length: Total polymer length is determined by adding the length of each individual microtubule of the spindle.

Microtubule polarity: For this analysis the spindle was split into a left and a right half, then the position of each microtubule end was determined and microtubule were assigned a polarity according to the microtubule end position that was closest to the chromosomes/spindle poles, with microtubules that had an end closer to of the left side being colored in blue and microtubules with ends closer to the right side in yellow. After this the number of microtubules for each category (blue and yellow) along the spindle axis in 500nm steps was quantified and the ratio of blue to yellow was calculated. A ratio of 1:1 was converted to a polarity of 0. Based on this the polarity along the spindle length was plotted.

Second harmonic generation imaging and two-photon florescence imaging

Simultaneous SHG imaging and TP imaging were constructed around an inverted microscope (Eclipse Ti, Nikon, Tokyo, Japan), with a Ti:sapphire pulsed laser (Mai-Tai, Spectra-Physics, Mountain View, CA) for excitation (850 nm wavelength, 80 MHz repetition

rate, ~70 fs pulse width), a commercial scanning system (DCS-120, Becker & Hickl, Berlin, Germany), and hybrid detectors (HPM-100–40, Becker & Hickl). The maximum scan rate of the DCS-120 is ~2 frames/s for a 512 × 512 imge. The excitation laser was collimated by a telescope to avoid power loss at the XY galvanometric mirror scanner and to fill the back aperture of a water-immersion objective (CFI Apo 40× WI, NA 1.25, Nikon). A half-wave plate (AHWP05M-980) and a quarter-wave plate (AQWP05M-980) were used in combination to achieve circular polarization at the focal plane, resulting in equal SHG of all orientations of microtubules in the plane, unbiased by the global rotation of the spindle, the spatial variation in the angle of the microtubules, and the local angular disorder of microtubules. Forward-propagating SHG was collected through an oil-immersion condenser (1.4, Nikon) with a 425/30 nm filter (FF01–425/30–25, Semrock). Two-photon fluorescence was imaged with a non-descanned detection scheme with an emission filter appropriate for green-fluorescent-protein (GFP)-labeled tubulin in *C. elegans* (FF01–520/5–25, Semrock, Rochester, NY).

Both pathways contained short-pass filters (FF01–650/SP-25, Semrock) to block the fundamental laser wavelength. Image analysis was performed with MATLAB (The MathWorks, Natick MA), and ImageJ (National Institutes of Health, Bethesda, MD.

Cell cycle stages were determined by “shape” and length of the spindle. Spindle length was measured on a single plane, from the outer edges of the tubulin signal. We monitored the spindles by light microscopy and acquired SHG and TP data at different stages throughout the initial stages of anaphase, during which the spindle still shortens. All stages shown in Figure 2 fall into the first ~80s of meiosis before the spindles start to elongate in agreement with Figure 1. For the plot, we grouped the spindles into 3 groups according to their length.

Statistical analysis.

The number of measured samples is indicated in the main text or figure legends, and for all measurements experiments were performed on a minimum of three or more different days. Unless otherwise stated statistical analysis was performed by using Student *t*-test assuming equal variance and two-tailed distribution. The data were analyzed and tested using Prism, Excel or MATLAB software. Correlation was tested using the Pearson’s Correlation Coefficient.

Statistics are presented as mean ± SEM, The significance level was set at $p < 0.05$, and displayed on figures with asterisks: * $p < 0.05$, ** $p < 0.01$, *** $p < 0.001$, **** $p < 0.0001$.

Supplementary Material

Refer to Web version on PubMed Central for supplementary material.

Acknowledgements

We are extremely grateful to Drs. Daniel Needleman and Che-Hang Yu for providing support and tools, as well as help with image analysis for the SHG and TP approach. The C. elegans strains were provided by the Caenorhabditis Genetics Center (CGC), which is funded by National Institutes of Health Office of Research Infrastructure Programs (P40 OD010440; University of Minnesota).

The Redemann lab was supported by 1R01GM144668-01 NIH NIGMS.

Data Availablity Statement

The data that support the findings of this study are available from the corresponding author upon reasonable request.

References

1. Mailhes JB, Carabatsos MJ, Young D, London SN, Bell M, Albertini DF. Taxol-induced meiotic maturation delay, spindle defects, and aneuploidy in mouse oocytes and zygotes. Mutat Res. 1999 Jan 25;423(1–2):79–90. [PubMed: 10029682]
2. Nakagawa S, FitzHarris G. Intrinsically Defective Microtubule Dynamics Contribute to Age-Related Chromosome Segregation Errors in Mouse Oocyte Meiosis-I. Curr Biol. 2017 Apr 3;27(7):1040–7. [PubMed: 28376326]
3. Holubcová Z, Blayney M, Elder K, Schuh M. Human oocytes. Error-prone chromosome-mediated spindle assembly favors chromosome segregation defects in human oocytes. Science. 2015 Jun 5;348(6239):1143–7. [PubMed: 26045437]
4. Schuh M, Ellenberg J. Self-organization of MTOCs replaces centrosome function during acentrosomal spindle assembly in live mouse oocytes. Cell. 2007 Aug 10;130(3):484–98. [PubMed: 17693257]
5. Albertson DG, Thomson JN. Segregation of holocentric chromosomes at meiosis in the nematode, Caenorhabditis elegans. Chromosome Res. 1993 May;1(1):15–26. [PubMed: 8143084]
6. Wolff ID, Tran MV, Mullen TJ, Villeneuve AM, Wignall SM. Assembly of Caenorhabditis elegans acentrosomal spindles occurs without evident microtubule-organizing centers and requires microtubule sorting by KLP-18/kinesin-12 and MESP-1. Mol Biol Cell. 2016 Oct 15;27(20):3122–31. [PubMed: 27559133]
7. Mullen TJ, Wignall SM. Interplay between microtubule bundling and sorting factors ensures acentriolar spindle stability during C. elegans oocyte meiosis. PLoS Genet. 2017 Sep 14;13(9):e1006986.
8. Muscat CC, Torre-Santiago KM, Tran MV, Powers JA, Wignall SM. Kinetochore-independent chromosome segregation driven by lateral microtubule bundles. eLife. 2015 May 30;4:e06462. [PubMed: 26026148]
9. Wignall SM, Villeneuve AM. Lateral microtubule bundles promote chromosome alignment during acentrosomal oocyte meiosis. Nat Cell Biol. 2009 Jul;11(7):839–44. [PubMed: 19525937]
10. Macaisne N, Bellutti L, Laband K, Edwards F, Pitayu-Nugroho L, Gervais A, et al. Synergistic stabilization of microtubules by BUB-1, HCP-1, and CLS-2 controls microtubule pausing and meiotic spindle assembly. eLife. 2023 Feb 17;12.
11. McNally K, Audhya A, Oegema K, McNally FJ. Katanin controls mitotic and meiotic spindle length. J Cell Biol. 2006 Dec 18;175(6):881–91. [PubMed: 17178907]
12. McNally FJ, Roll-Mecak A. Microtubule-severing enzymes: From cellular functions to molecular mechanism. J Cell Biol. 2018 Dec 3;217(12):4057–69. [PubMed: 30373906]
13. McNally K, Berg E, Cortes DB, Hernandez V, Mains PE, McNally FJ. Katanin maintains meiotic metaphase chromosome alignment and spindle structure in vivo and has multiple effects on microtubules in vitro. Mol Biol Cell. 2014 Apr;25(7):1037–49. [PubMed: 24501424]
14. Loughlin R, Wilbur JD, McNally FJ, Nédélec FJ, Heald R. Katanin contributes to interspecies spindle length scaling in Xenopus. Cell. 2011 Dec 9;147(6):1397–407. [PubMed: 22153081]
15. McNally KP, McNally FJ. The spindle assembly function of Caenorhabditis elegans katanin does not require microtubule-severing activity. Mol Biol Cell. 2011 May;22(9):1550–60. [PubMed: 21372175]
16. Srayko M, Buster DW, Bazirgan OA, McNally FJ, Mains PE. MEI-1/MEI-2 katanin-like microtubule severing activity is required for Caenorhabditis elegans meiosis. Genes Dev. 2000 May 1;14(9):1072–84. [PubMed: 10809666]

17. Nazockdast E, Redemann S. Mechanics of the spindle apparatus. Semin Cell Dev Biol. 2020 Nov;107:91–102. [PubMed: 32747191]

18. Herman JA, Miller MP, Biggins S. chTOG is a conserved mitotic error correction factor. eLife. 2020 Dec 30;9.

19. Yukawa M, Kawakami T, Pinder C, Toda T. Two XMAP215/TOG Microtubule Polymerases, Alp14 and Dis1, Play Non-Exchangeable, Distinct Roles in Microtubule Organisation in Fission Yeast. Int J Mol Sci. 2019 Oct 15;20(20).

20. Cassimeris L, Morabito J. TOGp, the human homolog of XMAP215/Dis1, is required for centrosome integrity, spindle pole organization, and bipolar spindle assembly. Mol Biol Cell. 2004 Apr;15(4):1580–90. [PubMed: 14718566]

21. Nakaseko Y, Goshima G, Morishita J, Yanagida M. M phase-specific kinetochore proteins in fission yeast: microtubule-associating Dis1 and Mtc1 display rapid separation and segregation during anaphase. Curr Biol. 2001 Apr 17;11(8):537–49. [PubMed: 11369198]

22. Byrnes AE, Slep KC. TOG-tubulin binding specificity promotes microtubule dynamics and mitotic spindle formation. J Cell Biol. 2017 Jun 5;216(6):1641–57. [PubMed: 28512144]

23. McHugh T, Welburn JPI. Potent microtubule-depolymerizing activity of a mitotic Kif18b-MCAK-EB network. J Cell Sci. 2023 Mar 1;136(5).

24. Steblyanko Y, Rajendraprasad G, Osswald M, Eibes S, Jacome A, Geley S, et al. Microtubule poleward flux in human cells is driven by the coordinated action of four kinesins. EMBO J. 2020 Dec 1;39(23):e105432. [PubMed: 33073400]

25. Bendre S, Rondelet A, Hall C, Schmidt N, Lin Y-C, Brouhard GJ, et al. GTSE1 tunes microtubule stability for chromosome alignment and segregation by inhibiting the microtubule depolymerase MCAK. J Cell Biol. 2016 Dec 5;215(5):631–47. [PubMed: 27881713]

26. Domnitz SB, Wagenbach M, Decarreau J, Wordeman L. MCAK activity at microtubule tips regulates spindle microtubule length to promote robust kinetochore attachment. J Cell Biol. 2012 Apr 16;197(2):231–7. [PubMed: 22492725]

27. Lindow N, Brünig FN, Dercksen VJ, Fabig G, Kiewisz R, Redemann S, et al. Semi-automatic stitching of filamentous structures in image stacks from serial-section electron tomography. J Microsc. 2021 Oct;284(1):25–44. [PubMed: 34110027]

28. Lindow N, Redemann S, Brünig F, Fabig G, Müller-Reichert T, Prohaska S. Quantification of three-dimensional spindle architecture. Methods Cell Biol. 2018;145:45–64. [PubMed: 29957215]

29. Redemann S, Weber B, Möller M, Verbavatz J-M, Hyman AA, Baum D, et al. The segmentation of microtubules in electron tomograms using Amira. Methods Mol Biol. 2014;1136:261–78. [PubMed: 24633801]

30. Redemann S, Müller-Reichert T. Correlative light and electron microscopy for the analysis of cell division. J Microsc. 2013 Aug;251(2):109–12. [PubMed: 23734865]

31. Kim W, Underwood RS, Greenwald I, Shaye DD. OrthoList 2: A New Comparative Genomic Analysis of Human and Caenorhabditis elegans Genes. Genetics. 2018 Oct;210(2):445–61. [PubMed: 30120140]

32. Lantzsch I, Yu C-H, Chen Y-Z, Zimyanin V, Yazdkhasti H, Lindow N, et al. Microtubule reorganization during female meiosis in C. elegans. eLife. 2021 Jun 11;10.

33. McNally KP, Panzica MT, Kim T, Cortes DB, McNally FJ. A novel chromosome segregation mechanism during female meiosis. Mol Biol Cell. 2016 Aug 15;27(16):2576–89. [PubMed: 27335123]

34. Yang H, Mains PE, McNally FJ. Kinesin-1 mediates translocation of the meiotic spindle to the oocyte cortex through KCA-1, a novel cargo adapter. J Cell Biol. 2005 May 9;169(3):447–57. [PubMed: 15883196]

35. Yu C-H, Redemann S, Wu H-Y, Kiewisz R, Yoo TY, Conway W, et al. Central-spindle microtubules are strongly coupled to chromosomes during both anaphase A and anaphase B. Mol Biol Cell. 2019 Sep 1;30(19):2503–14. [PubMed: 31339442]

36. Zimyanin V, Magaj M, Yu C-H, Gibney T, Mustafa B, Horton X, et al. Lack of chromokinesin Klp-19 creates a more rigid midzone and affects force transmission during anaphase in C. elegans. BioRxiv. 2023 Oct 26;

37. Yu C-H, Langowitz N, Wu H-Y, Farhadifar R, Brugues J, Yoo TY, et al. Measuring microtubule polarity in spindles with second-harmonic generation. Biophys J. 2014 Apr 15;106(8):1578–87. [PubMed: 24739157]
38. Redemann S, Lantzsch I, Lindow N, Prohaska S, Srayko M, Müller-Reichert T. A Switch in Microtubule Orientation during C. elegans Meiosis. Curr Biol. 2018 Sep 24;28(18):2991–2997.e2. [PubMed: 30197085]
39. Nannas NJ, O'Toole ET, Winey M, Murray AW. Chromosomal attachments set length and microtubule number in the Saccharomyces cerevisiae mitotic spindle. Mol Biol Cell. 2014 Dec 15;25(25):4034–48. [PubMed: 25318669]
40. Kletter T, Reusch S, Cavazza T, Dempewolf N, Tischer C, Reber S. Volumetric morphometry reveals spindle width as the best predictor of mammalian spindle scaling. J Cell Biol. 2022 Jan 3;221(1).
41. Hara Y, Kimura A. An allometric relationship between mitotic spindle width, spindle length, and ploidy in Caenorhabditis elegans embryos. Mol Biol Cell. 2013 May;24(9):1411–9. [PubMed: 23468523]
42. Hunter AW, Caplow M, Coy DL, Hancock WO, Diez S, Wordeman L, et al. The kinesin-related protein MCAK is a microtubule depolymerase that forms an ATP-hydrolyzing complex at microtubule ends. Mol Cell. 2003 Feb;11(2):445–57. [PubMed: 12620232]
43. Connolly AA, Sugioka K, Chuang C-H, Lowry JB, Bowerman B. KLP-7 acts through the Ndc80 complex to limit pole number in C. elegans oocyte meiotic spindle assembly. J Cell Biol. 2015 Sep 14;210(6):917–32. [PubMed: 26370499]
44. Gigant E, Stefanutti M, Laband K, Gluszek-Kustusz A, Edwards F, Lacroix B, et al. Inhibition of ectopic microtubule assembly by the kinesin-13 KLP-7 prevents chromosome segregation and cytokinesis defects in oocytes. Development. 2017 May 1;144(9):1674–86. [PubMed: 28289130]
45. Goshima G, Wollman R, Stuurman N, Scholey JM, Vale RD. Length control of the metaphase spindle. Curr Biol. 2005 Nov 22;15(22):1979–88. [PubMed: 16303556]
46. Wollman R, Cytrynbaum EN, Jones JT, Meyer T, Scholey JM, Mogilner A. Efficient chromosome capture requires a bias in the "search-and-capture" process during mitotic-spindle assembly. Curr Biol. 2005 May 10;15(9):828–32. [PubMed: 15886100]
47. Lacroix B, Letort G, Pitayu L, Sallé J, Stefanutti M, Maton G, et al. Microtubule Dynamics Scale with Cell Size to Set Spindle Length and Assembly Timing. Dev Cell. 2018 May 21;45(4):496–511.e6. [PubMed: 29787710]
48. Brenner S The genetics of Caenorhabditis elegans. Genetics. 1974 May;77(1):71–94. [PubMed: 4366476]
49. Timmons L, Fire A. Specific interference by ingested dsRNA. Nature. 1998 Oct 29;395(6705):854. [PubMed: 9804418]
50. Fraser AG, Kamath RS, Zipperlen P, Martinez-Campos M, Sohrmann M, Ahringer J. Functional genomic analysis of C. elegans chromosome I by systematic RNA interference. Nature. 2000 Nov 16;408(6810):325–30. [PubMed: 11099033]
51. Woog I, White S, Büchner M, Srayko M, Müller-Reichert T. Correlative light and electron microscopy of intermediate stages of meiotic spindle assembly in the early Caenorhabditis elegans embryo. Methods Cell Biol. 2012;111:223–34. [PubMed: 22857931]
52. Pelletier L, O'Toole E, Schwager A, Hyman AA, Müller-Reichert T. Centriole assembly in Caenorhabditis elegans. Nature. 2006 Nov 30;444(7119):619–23. [PubMed: 17136092]
53. Muller-Reichert T, Srayko M, Hyman A, O'Toole ET, McDonald K. Correlative light and electron microscopy of early Caenorhabditis elegans embryos in mitosis. Methods Cell Biol. 2007;79:101–19. [PubMed: 17327153]
54. Kremer JR, Mastronarde DN, McIntosh JR. Computer visualization of three-dimensional image data using IMOD. J Struct Biol. 1996;116(1):71–6. [PubMed: 8742726]
55. Stalling D, Westerhoff M, Hege HC. Amira: a highly interactive system for visual data analysis. In: Hansen CD, Johnson CR, editors. The Visualization Handbook. Elsevier; 2005. p. 749–767.
56. Redemann S, Baumgart J, Lindow N, Shelley M, Nazockdast E, Kratz A, et al. C. elegans chromosomes connect to centrosomes by anchoring into the spindle network. Nat Commun. 2017 May 11;8:15288. [PubMed: 28492281]

57. Weber B, Greenan G, Prohaska S, Baum D, Hege H-C, Müller-Reichert T, et al. Automated tracing of microtubules in electron tomograms of plastic embedded samples of Caenorhabditis elegans embryos. J Struct Biol. 2012 May;178(2):129–38. [PubMed: 22182731]

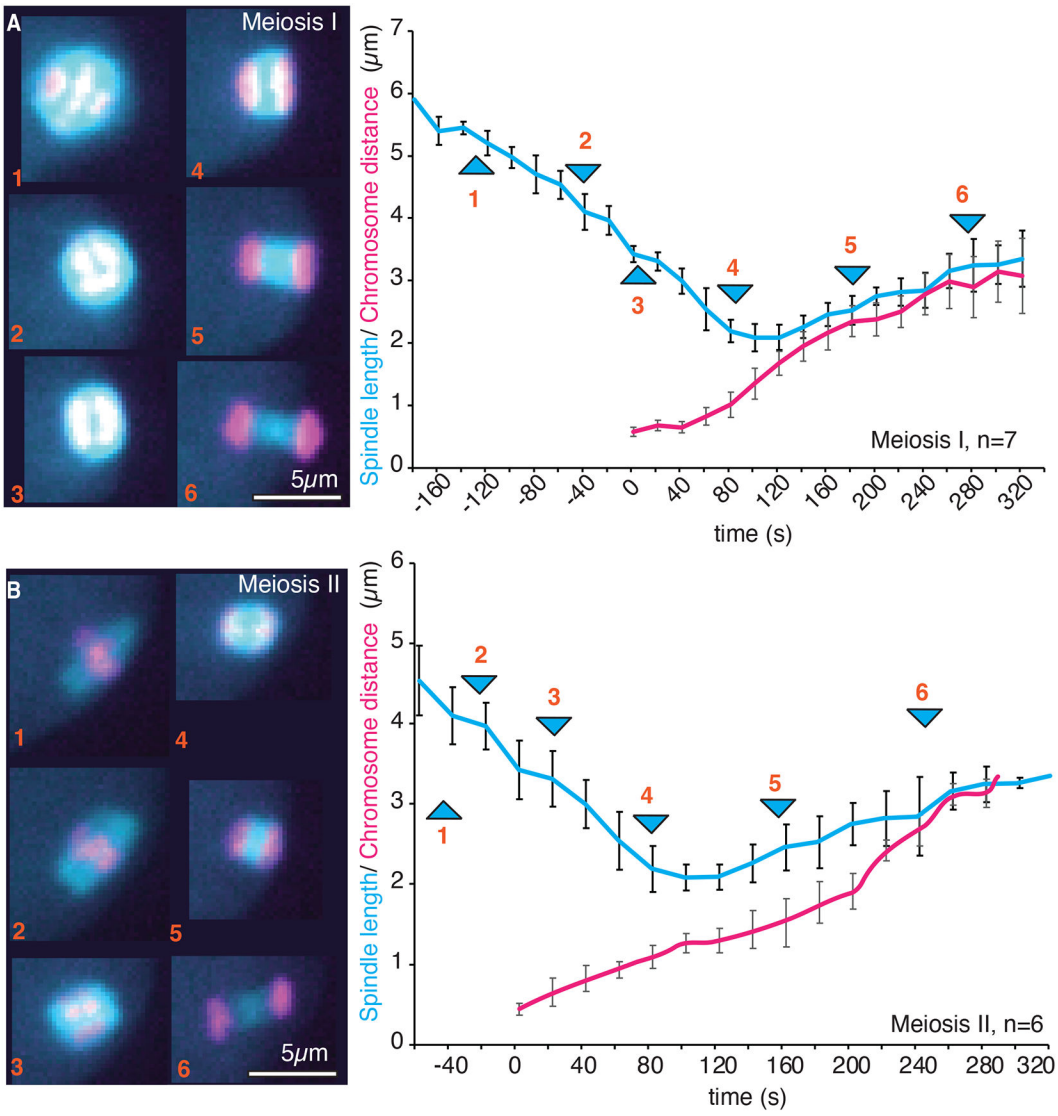

Figure1. Meiotic divisions are accompanied by rearrangement of the spindle

A. Left panel. Fluorescent confocal images of different stages of *C. elegans* Meiosis I division labelled with GFP-Tubulin and Cherry-Histone. Right panel: Plot of the spindle length (blue) and chromosome distance (red) changes during Meiosis I. Arrows with numbers correspond to the stages of division shown in the images in the left panel. The timepoint '0' corresponds to anaphase onset, the first timepoint (frame) with detectable chromosome segregation. **B.** Left panel. Fluorescent confocal images of different stages of *C. elegans* Meiosis II Right panel: Plot of the spindle length (blue) and chromosome distance (red) changes during Meiosis II division. Arrows with numbers correspond to the stages of division shown in the images in the left panel. Scale bars are 5μm, error bars are sem.

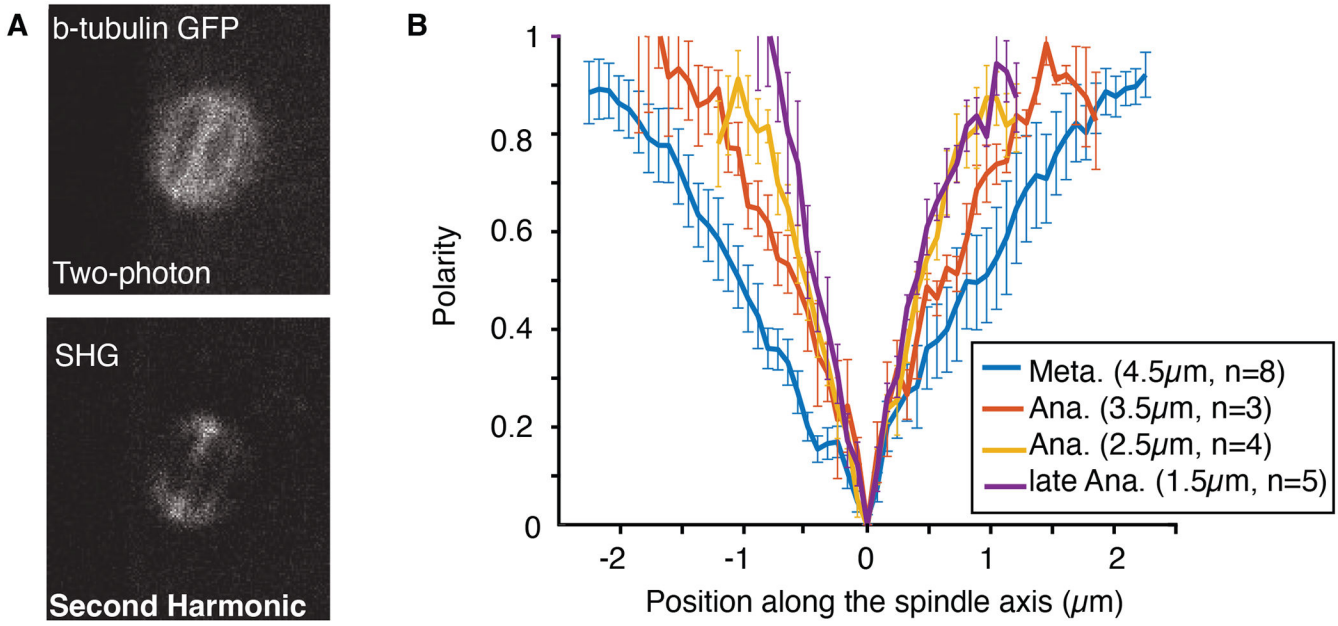

Figure 2. Microtubule overlap in the midzone is reduced during chromosome segregation.

A. Two-photon fluorescence image of GPF labeled β-tubulin (top) and second harmonic image (bottom) of a representative Meiosis I metaphase spindle showing overall microtubules localization (top) and their polarity (bottom): low signal indicating in SHG corresponding to antiparallel microtubule. **B.** Average polarity plots of microtubules in the spindle throughout metaphase and anaphase of meiosis I divisions obtained by the combination of SHG and TP microscopy. 0 on the x-axis represents the spindle center. Sample number is indicated in the legend and example images of spindles at the corresponding stage are shown. Error bars are sem.

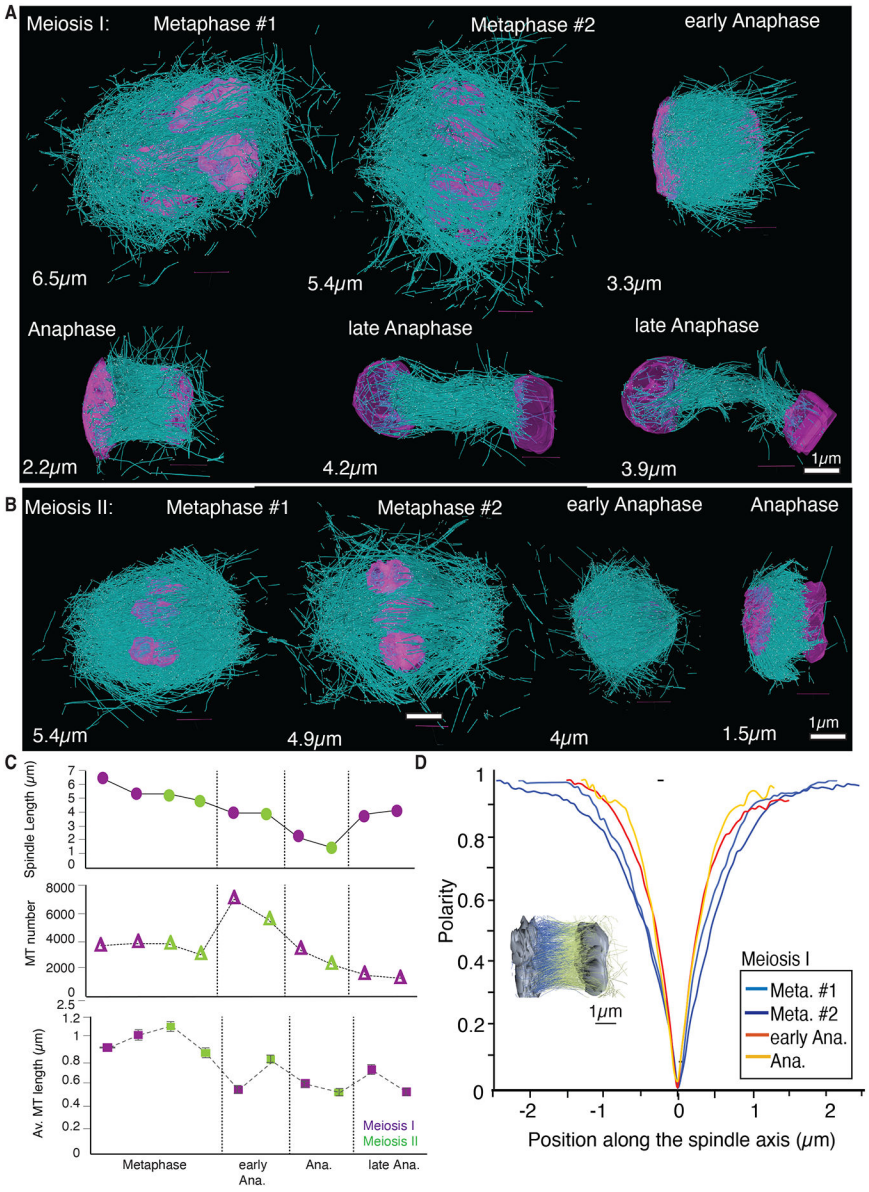

Figure 3. Ultrastructural TEM reconstructions reveal the structure of meiotic spindles at the resolution of single microtubules.

A-B. 3D tomographic reconstructions of different stages of Meiosis I (A) and Meiosis II (B) obtained by electron tomography. Scale bar is 1μm **C.** Plots showing different parameters of spindles determined by electron tomography in Meiosis I (purple) and Meiosis II (green) at stages shown in A-B, top: individual measurements of spindle length, middle: microtubule numbers of the individual spindles, bottom: Average microtubule (MT) length at the different stages, error bars are sem **D.** Microtubule polarity plot based on the ultrastructural TEM reconstruction to show reduction of microtubule overlap with meiosis progression. 0 on the x-axis represents the spindle center. Average spindle length is indicated in the legend (n=1 for each spindle).

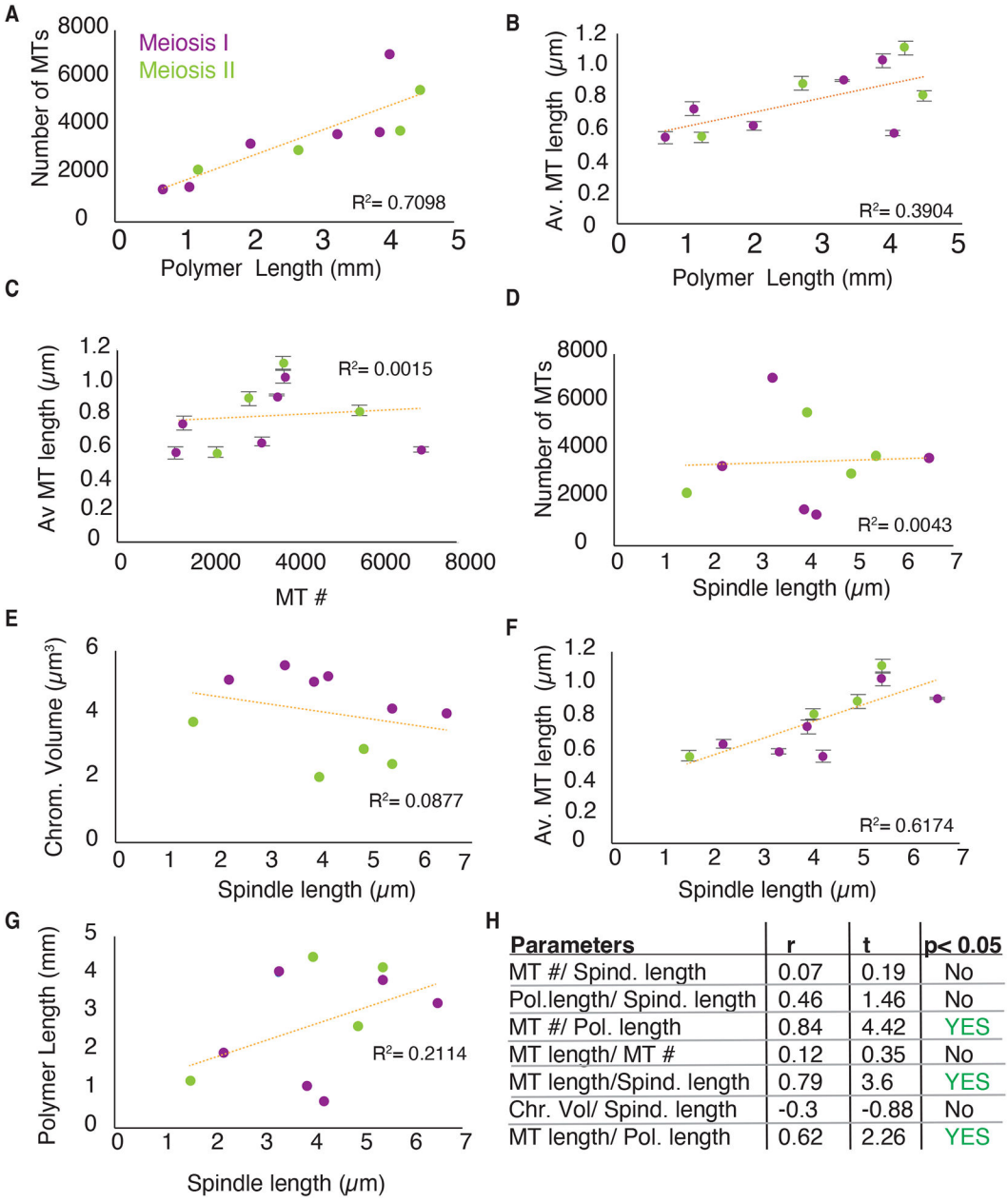

H

Parameters	r	t	p< 0.05
MT #/ Spind. length	0.07	0.19	No
Pol.length/ Spind. length	0.46	1.46	No
MT #/ Pol. length	0.84	4.42	YES
MT length/ MT #	0.12	0.35	No
MT length/Spind. length	0.79	3.6	YES
Chr. Vol/ Spind. length	-0.3	-0.88	No
MT length/ Pol. length	0.62	2.26	YES

Figure 4.

Microtubule length correlates with spindle length A-F. Correlation plots demonstrating relationship between different parameters of spindles at different stages throughout Meiosis I (purple) and Meiosis II (green): Number of microtubules, average microtubule length, total Polymer length (added length of each individual microtubule in the spindle), Spindle length and Chromosome volume. **H**. Table showing correlation coefficient r, t and p-value significance for the analysis shown in **A-F**. Error bars for average microtubule length are sem.

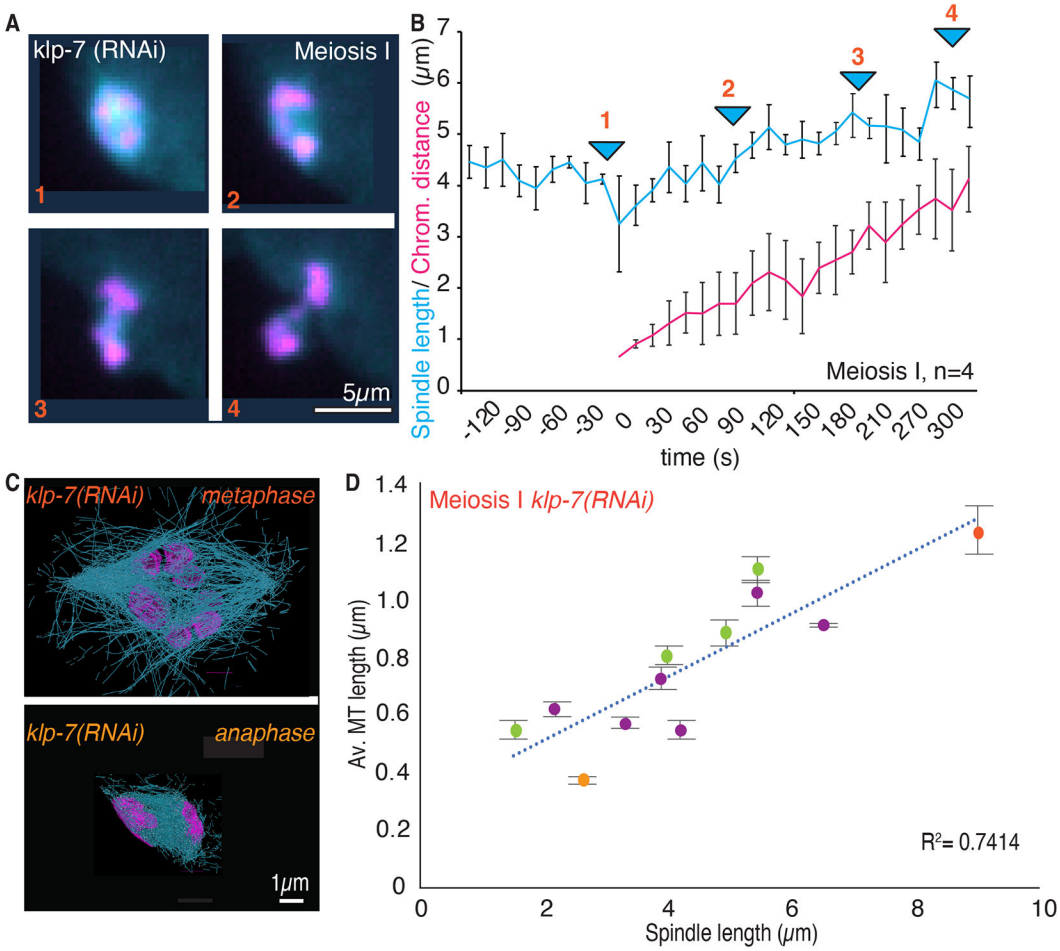

Figure 5. Microtubule and Meiotic spindle length are both increased in meiosis I metaphase spindles after *klp-7 (RNAi)*.

A. Fluorescent confocal images of different stages of meiosis I division in *klp-7 (RNAi)* treated embryos labelled with GFP-Tubulin and Cherry-Histone. **B**. Plot of the spindle length (blue) and chromosome distance (red) changes during meiosis I division. Arrows with numbers correspond to the stages of division shown in the images in the left panel. **C.** Reconstructions of microtubules in *klp-7 (RNAi)* meiotic spindles at metaphase (upper panel) and anaphase (lower panel) of the C. elegans one-cell embryo obtained by 3D electron tomography. **D.** Correlation plot comparing relationship of average microtubule length and spindle length in *klp-7 (RNAi)* spindles at metaphase (red) and anaphase (orange) shown in relation to the same values in wt meiosis I (purple) and II (green). Scale bars are 5μm, error bars are sem.